Microstructure evolution during the extrusion of a 6351 aluminum alloy tube

http://dx.doi.org/10.1590/0370-44672018720174

Wei Tsu Jinan[1,2]
https://orcid.org/0000-0002-2023-2787
Angelo Fernando Padilha[1,3]
https://orcid.org/0000-0002-5494-9137

[1]Universidade de São Paulo - USP, Escola Politécnica, Departamento de Engenharia Metalúrgica e de Materiais, São Paulo - São Paulo – Brasil.

E-mails: [2]yatowei@hotmail.com, [3]padilha@usp.br

Abstract

The aluminum alloy AA 6351 is a precipitation hardened alloy of the Al-Mg-Si system, additionally containing Mn and Fe. In this study, the microstructural characterization during processing of a thick wall extruded AA 6351 tube was carried out. Several complementary techniques for microstructural characterization were used, such as polarized light optical microscopy, scanning electron microscopy, energy dispersive X-ray spectroscopy, backscattered electron diffraction, X-ray diffraction, hardness and electrical conductivity measurements. The main characteristics of the grains and precipitates were analyzed. After solidification, the presence of a relatively homogeneous grain distribution with an average diameter of about 100 μm and an intermetallic phase with elongated morphology rich in Al, Fe, Mn and Si was observed. During extrusion, the initial grain size was reduced to about one-fifth of the initial diameter and the elongated phase, probably α-Al(Fe,Mn)Si, was fractured and redistributed and the resulting fragments were aligned in the extrusion direction. A peripheral coarse grain zone was detected and analyzed near the outer and inner surfaces of the tube.

Keywords: alloy AA 6351, extrusion, microstructure, peripheral coarse grain zone.

1. Introduction

Aluminum alloy 6351 is a precipitation hardened alloy of the Al-Si-Mg system, containing about 2.5 mass % of solute. In addition to Si (0.7 to 1.3%), Mg (0.4 to 0.8%) and Mn (0.4 to 0.8%), this alloy frequently contains Fe (max. 0.5%) in its chemical composition. In the artificially aged condition (T6), the alloy 6351 has moderate mechanical strength, with a yield limit of about 285 MPa. This is more than twice that of non-heat-treated aluminum alloys, such as AA 3003 and AA 5052 in the annealed condition, but lower than that of the AA 2024 and AA 7075 alloys, which may be present after aging, with a yield limit of about 500 MPa. On the other hand, the ductility and the formability of the 6351 alloy are significantly higher than that of the alloys 2024 and 7075, and it is less susceptible to stress corrosion cracking. The superior plasticity of the AA 6351 allows the production of extruded products such as bars, wires, profiles, and tubes (Davis, 2001). Due to its attractive combination of mechanical properties, formability, corrosion resistance, machinability, and weldability, the AA 6351 alloy finds several applications in the construction of ships, trucks and buses, as well as in oil and gas pipelines (Reddy *et al.*, 2014). The occurrence of a peripheral coarse grain zone (PCG) in extruded aluminum profiles is a relatively frequent event (Van Geertruyden *et al.*, 2005) (Eivani; Zhou; Duszczyk, 2016). This zone is a surface defect that has negative consequences on mechanical strength, fatigue strength, machinability, corrosion resistance, resistance to stress corrosion cracking, anodized surface quality, aesthetic appearance, and susceptibility to formation during the subsequent plastic deformation of a superficial defect known as orange peel. In spite of this, no systematic study on the microstructural evolution during tube extrusion of 6351 aluminum alloy has been found in the technical literature.

The general objective of this research was to study, with the aid of several complementary techniques of microstructural characterization, the microstructural modifications that occur during the extrusion of a thick wall tube of the AA 6351 aluminum alloy. The main techniques used were optical microscopy, polarized light optical microscopy, scanning electron microscopy, chemical microanalysis through energy dispersive X-ray spectroscopy, microtexture and mesotexture with the aid of backscattered electron diffraction, and X-ray diffraction, in addition to hardness and electrical conductivity measurements.

2. Material and methods

Initially, the 228.6 mm diameter billet that gave origin to the extruded tube had its microstructure characterized. Then, an extruded tube with an internal diameter of 175 mm and wall thickness of 22.5 mm was analyzed. The chemical composition (mass %) of the 6351 alloy was determined by optical emission spectrometry (OES): 0.98Si; 0.224Fe; 0.032Cu; 0.449Mn; 0.716Mg; 0.062Zn; 0.022Ti. The chemical composition was in agreement with the specification for all elements and presents a relatively low Mg/Si (0.731) ratio (Zhu; Couper; Dahle, 2011). Samples were prepared for microscopy analysis as follows: i) grinding with silicon carbide (SiC) grades 220, 400, 800 and 1200; ii) polishing with alumina suspension, followed by polishing with colloidal silica; and iii) anodization with 1.8% HBF_4 solution (Barker's solution) using a 20 V source. Next, samples were analyzed under polarized light optical microscopy. With the aid of the scanning electron microscope, images were made using secondary and backscattered electrons, X-ray spectroscopy analyses were performed by energy dispersion and backscattered electron diffraction analysis (EBSD) were performed. For the EBSD analysis, the mechanically polished samples were additionally electrolytically polished using a 30% (volume %) solution of perchloric acid in ethanol, with an applied voltage of 30 V during 30 seconds. For X-ray diffraction, the samples were mechanically polished and analyzed with Cu-Kα1 radiation. Vickers hardness measurements were performed with a load of 200 g. The hardness measurements were made both in the longitudinal and transverse section, in the center and in the inner and outer tube peripheries. All electrical conductivity measurements were carried out with a digital device that works based on the eddy current phenomena.

3. Results and discussion

3.1 Microstructural characterization of the billet prior to extrusion

Samples taken from the center and near the billet surface were analyzed using polarized light optical microscopy (PLOM) and scanning electron microscopy (SEM). SEM analyses using backscattered electron diffraction (BSED) were also carried out. Figure 1 presents the results obtained using PLOM on the billet after solidification. The micrographs show a microstructure with a relatively homogeneous grain size distribution, with an average diameter of about 100 µm and a small grain size variation between the center and the border of the billet (the particle size at the center of the ingot is slightly finer). There is also an elongated, but not continuous phase with a higher incidence at grain boundaries. Figure 2 shows micrographs obtained with SEM after solidification. With the help of SEM, it was possible to confirm the observations made with PLOM and to see in great detail the morphology of the second phase formed during solidification, confirming that the microstructural differences between the center and the borders of the billet are not significant. The next step of the analysis was performed using SEM-EDS. Several elongated particles were analyzed and the following average composition (mass %) was detected: Al = 73.3%; Fe = 10.3%; Mn = 9.1%; Si = 6.3% and Mg = 1.0%.

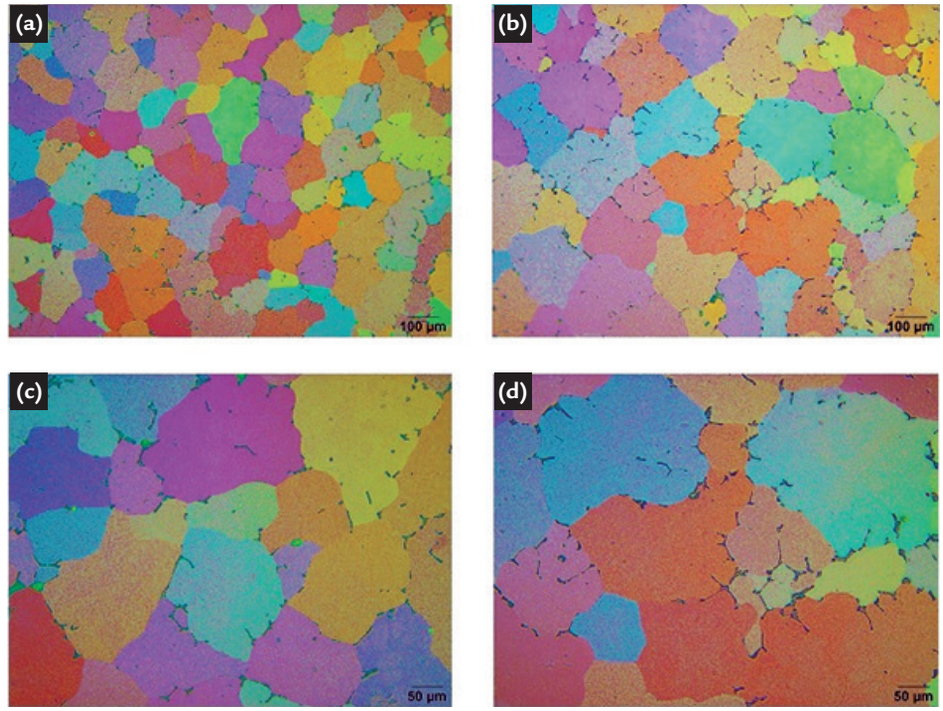

Figure 1
Micrographs obtained using polarized light optical microscopy following anodization with Barker's reagent at the center (a, b) and at the edge (c, d) of the billet after solidification.

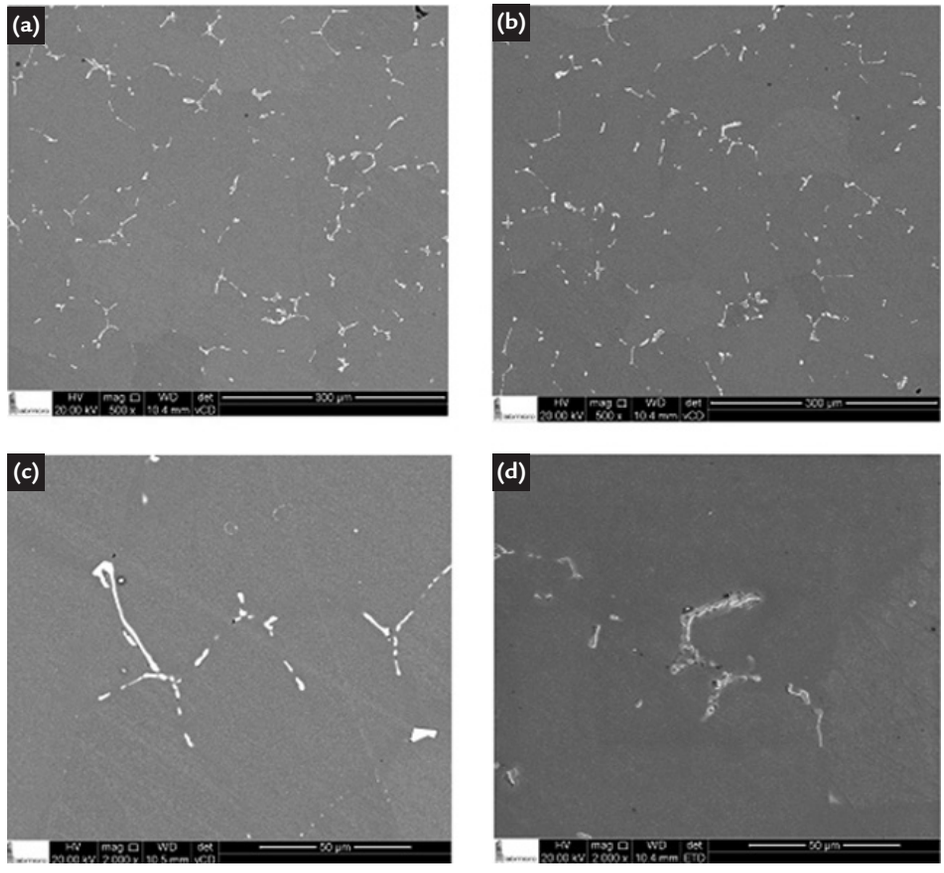

Figure 2
Micrographs obtained with scanning electron microscopy using BSE at the center (a, b) and at the edge (c, d) of the billet after solidification.

The average of the electrical conductivity measured in 10 points of the billet was 40.5% IACS, equivalent to 23.5 mS/m. The average Vickers hardness was 121.2 HV. The electrical conductivity and Vickers hardness found in literature for this alloy are 26.2 mS/m and 107 HV, respectively (DAVIS, 2001). The X-ray pattern showed typical aluminum peaks and almost no peaks related to the precipitates, which is reasonable for a low volumetric second phase fraction. Although very accurate, the X-ray diffraction technique has a poor detection limit, around 1% to 2% volume fraction (Cullity, 1978).

In synthesis, the solidification of the alloy begins with the formation of dendrites of a solid solution Al-Mg-Si. The remaining liquid is enriched in Fe, Mn, Si, and Mg. The low solubility of Fe, Si, and Mn in Al leads to the formation of the second phase in the interdendritic regions. In addition, the (Fe+Mn) content of the alloy is comparable to the Mg content, so the presence of numerous second phase particles containing Fe and Mn is not surprising. The coarse and elongated particles are hardly

dissolved during the homogenization heat treatment prior to extrusion. Finally, no evidence of microsegregation was found in the SEM images with backscattered electrons, but this is also due to the small differences in the atomic number between Al and Mg and Si and the low solid solubility of Fe and Mn in Al.

3.2 Microstructural characterization of the extruded tube

Electrical conductivity measurements were performed at 4 points in the cross section and at 10 points on the outer surface along the length of the tube. Measurements were additionally taken in 6 more randomly chosen points, comprising 20 measurement positions. The average of the electrical conductivity measurements performed at 20 positions was 47.4% IACS (27.5 mS/m). The electrical conductivity value of the AA 6351 alloy in the T6 (solution annealed and artificially aged) condition found in literature is 46% IACS (Davis, 2001). The measured hardness was 98 HV, whereas that in the literature for the AA 6351 alloy in the T6 condition is 100 HV (Davis, 2001). Hardness variation along the cross section was not significant, the outer periphery being slightly harder than the inner periphery. The characteristics of the precipitates were studied with the aid of SEM and EDS. Figure 3 shows larger, aligned precipitates with irregular and partially faceted interfaces.

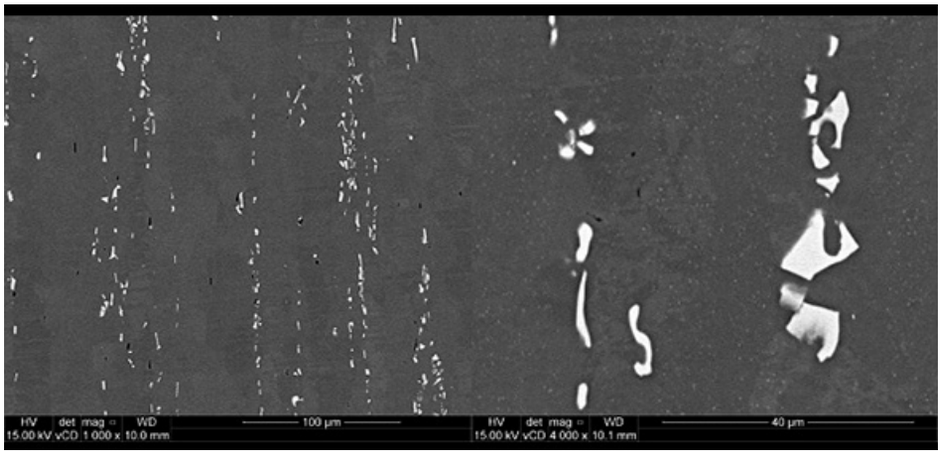

Figure 3
Images of the largest precipitates obtained with scanning electron microscopy using BSE with two magnifications.

A detailed analysis of the microstructure using SEM/EDS revealed the presence of three types of particles. The larger particles already mentioned and shown in Figure 3 contained Al, Fe, Mn, and Si and are probably particles of the α-Al(FeMn)Si phase (Priya *et al.*, 2016). The presence of these particles is justified by the relatively high concentration of (Fe+Mn+Si) in the alloy (1.653%) and low solubility of these elements in aluminum, especially iron and silicon. The volumetric fraction of these particles is not very sensitive to thermal treatments. They are originated by the fragmentation and orientation in the extrusion direction of the elongated particles observed in the billet after the solidification condition. The dark, large and much less frequent particles were rich in Al, Mg, Si, and O. These particles, which are probably oxides, are rare and not very sensitive to heat treatments. However, the light and very fine particles were not large enough for accurate EDS analysis, but are supposedly rich in (Mg+Si) that are sensitive to heat treatments and related to the precipitation hardening process of the alloy.

The presence (see Figure 4) of peripheral coarse grains (PCG) near the outer and inner surfaces of the tube was first detected with PLOM. The thickness of the coarse grain layer varied from 200 to 600 µm. The formation of PCG is strongly linked to the rate of deformation (Van Geertruyden *et al.*, 2005). During extrusion, the outer and inner walls are regions with higher deformation rates. Therefore, in these regions, accumulation of stored energy as crystalline defects (mainly dislocations) and increase in temperature favors recrystallization (Van Geertruyden *et al.*, 2005) (Eivani, Zhou, Duszczyk, 2016).

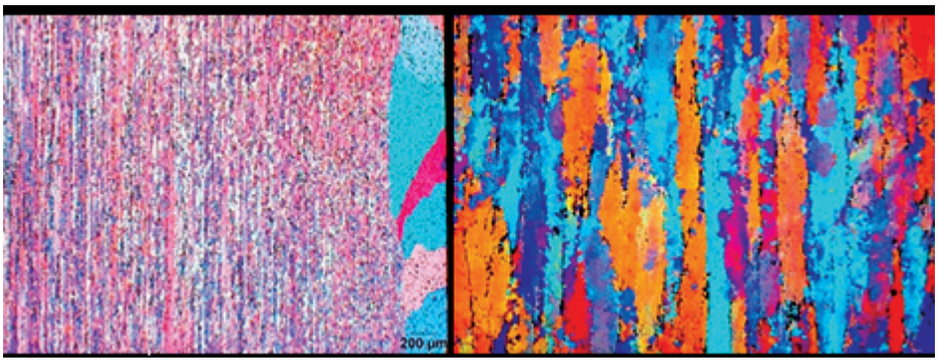

Figure 4
Micrographs obtained using polarized light optical microscopy after anodization with Barker reagent: external periphery (20X magnification; left); central region of the thickness (50X magnification; right).

EBSD was used to detect possible crystallographic preferences (microtexture), orientation differences between neighboring micro-regions (mesotexture) and determination of mean grain size in three cross-sec-

tional regions of the tube: outer border, central, and inner border. Some results concerning EBSD analysis are presented in Figure 5. The colors (each color represents a crystallographic orientation) on the left-hand side show that texture varies along the cross-section of the tube. On the right-hand side, analysis of the degree of misorientation between grain or sub-grain boundaries (mesotexture) are presented. The grain boundaries and the sub-grain boundaries were divided into three classes of orientation differences: between 2 and 5° (red lines); between 5 and 15° (green lines) and between 15 and 180° (blue lines). Table 1 shows the mesotexture results obtained in three regions of the tube: external surface, central region, and inner surface. The analysis of the results presented in Table 1 revealed that in the inner and outer border of the tube, 65% of the boundaries were high angle grain boundaries (HAGB), whereas in the central region only 42% were HAGB. In addition, the presence of low angle grain boundaries (LAGB) was more pronounced in the central region. This suggests that the internal and external borders are more recrystallized (higher recrystallized volume fraction) than the center of the sample, although the measurements of hardness and electrical conductivity in these regions did not reveal significant differences. In the outer surface of the tube, the degree of deformation (driving force for recrystallization) and the temperature increase due to the friction during extrusion are larger. Both factors contribute to a faster recrystallization rate and consequently to greater softening.

The average grain sizes at the outer border, center, and inner border were 16.7 µm, 34.7 µm and 20.5 µm, respectively. This suggests a greater accumulation of crystalline defects in these regions during extrusion, with the formation of a larger number of recrystallization nuclei and smaller recrystallized grain size in the external and internal regions in comparison with that at the center of the tube wall. Near the surface, grain size is larger and there is a larger fraction of low-angle grain boundaries or sub-boundaries.

The X-ray diffraction results showed typical aluminum peaks and other much less intense peaks that can be attributed to the α-Al(Fe,Mn)Si and Mg_2Si phases.

In synthesis, in the microstructure of the extruded tube, it is possible to state that during extrusion, there was fragmentation and alignment in the direction of extrusion of the primary precipitates (formed during the solidification). There was also significant grain refining and formation of a coarse-grained peripheral zone.

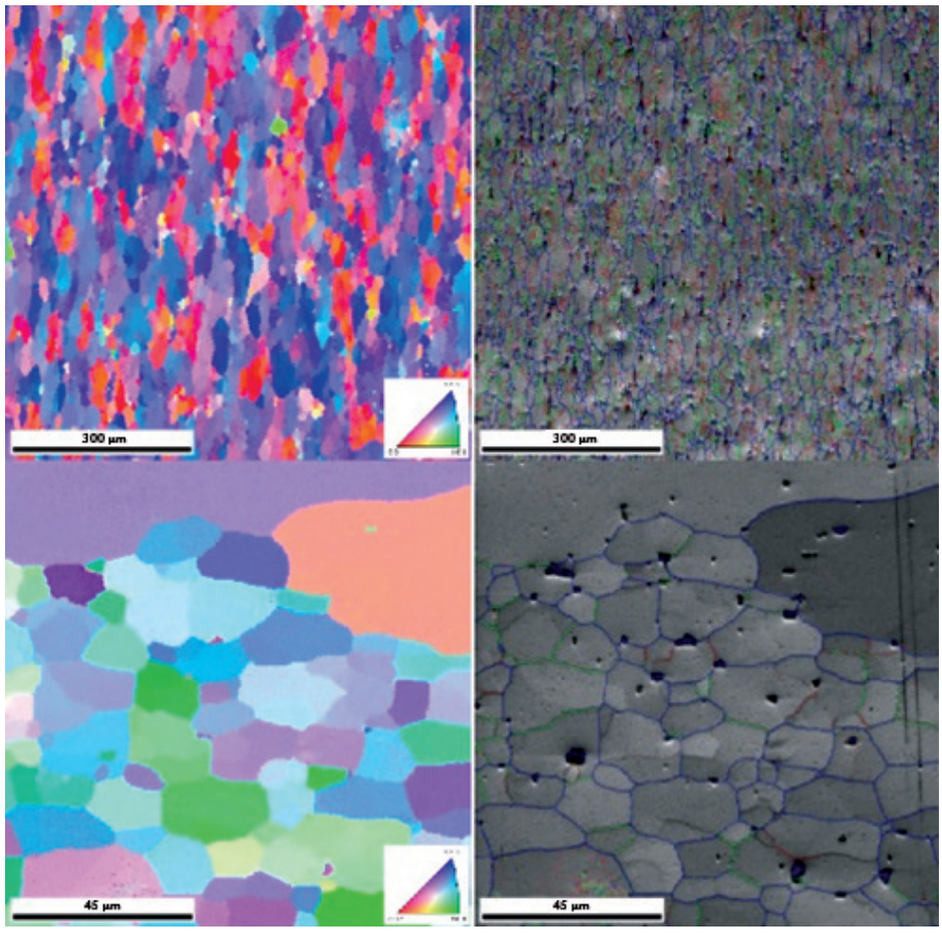

Figure 5
EBSD maps of two regions of the tube cross-section: central region (top image) and inner surface (bottom image). The image magnifications are not the same.

Table 1
Analysis of the misorientation between boundaries (mesotexture) in three regions of the cross-section of the tube: external surface; central region and inner surface.

Misorientation range	Boundary Color	External surface	Center	Internal surface
2 to 5°	Red	20.3	31.4	15.5
5 to 15°	Green	14.2	26.5	19.6
15 to 180°	Blue	65.4	42.1	64.9

4. Conclusions

The obtained results allow us to conclude that:

a) The billet after solidification shows a microstructure of equiaxed grains with relatively homogeneous size distribution and average diameter of about 100 µm. An intermetallic phase with elongated morphology and rich in aluminum, iron, manganese, and silicon is detected, often located at the grain boundaries, but also in the interior of the grains.

b) During extrusion, the initial grain size is reduced to about one-fifth (to about 20 µm) of that observed after solidification and the elongated phase containing Al-Fe-Mn-Si is fragmented and redistributed. These fragments are preferentially aligned in the extrusion direction.

c) No macroscopic extrusion defects are detected. Two types of precipitates are seen: one rich in Mg and Si (probably Mg_2Si) and one rich in Al, Mn, Fe, and Si, probably α-Al(Fe,Mn)Si. The precipitate distribution is almost invariable along the thickness. However, grain size distribution is heterogeneous, with grain orientation preference (crystallographic texture) and with low angle sub-grain boundary fraction (mesotexture).

d) Peripheral coarse grain (PCG) zones are detected near the outer and inner surfaces of the tube. The thickness of the coarse grain layer varies from 200 to 600 µm. The occurrence of these coarse grain zones can be explained by the higher concentrations of dislocations and higher temperature in these regions during extrusion.

References

CULLITY, B. D. ***Elements of x-ray diffraction.*** (2nd. Ed.). Reading (MA, USA): Addison-Wesley, 1978.

DAVIS, J. R. Aluminum and aluminum alloys. ***Light Metals and alloys,*** v. 3, p. 351–416, 2001.

EIVANI, A. R., ZHOU, J., DUSZCZYK, J. Mechanism of the formation of peripheral coarse grain structure in hot extrusion of Al-4.5Zn-1Mg. ***Philosophical Magazine,*** v. 96, n. 12, p. 1188–1196, 2016.

PRIYA, P., JOHNSON, D. R., KRANE, M. J. N. Numerical study of microstructural evolution during homogenization of Al-Si-Mg-Fe-Mn alloys. ***Metallurgical and Materials Transactions A,*** v. 47, n. 9, p. 4625-4639, 2016.

REDDY, M. V. N., REDDY, M. N., KUMAR, K. V., GARRE, P. Experimental investigation of tensile strength on Al 6361 to the aerospace structural applications. ***International Journal of Mechanical Engineering and Technology (IJMET),*** v. 5, n. 2, p. 110–114, 2014.

VAN GEERTRUYDEN, W. H., BROWNE, H. M., MISIOLEK, W. Z., WANG, P. T. Evolution of surface recrystallization during indirect extrusion of 6xxx aluminum alloys. ***Metallurgical and Materials Transactions A,*** v. 36, n. 4, p. 1049–1056, 2005.

VERMOLEN, F., VUIK, K., van der ZWAAG, S. A mathematical model for the dissolution kinetics of Mg_2Si-phases in Al-Mg-Si alloys during homogenisation under industrial conditions. ***Materials Science and Engineering A,*** v. 254, n. 1-2, p. 13-22, 1998.

YOSHIKAWA, D. S., CARVALHO, L. G., PLAUT, R. L., PADILHA, A. F. Effect of casting mode and thermal treatments on the electrical conductivity of the AA4006 aluminum alloy. ***REM-International Engineering Journal,*** v. 70, n. 4, p. 471-476, 2017.

ZHU, H., COUPER, M. J., DAHLE, A. K. Effect of process variables on Mg-Si particles and extrudability of 6xxx series aluminum extrusions. ***JOM,*** v. 63, n. 11, p. 66–71, 2011.

Received: 14 December 2018 - Accepted: 15 April 2019.